A New Method for Calculating Instantaneous Atmospheric Heat Transport

TYLER COX,[a,e] AARON DONOHOE,[b] KYLE C. ARMOUR,[c,a] GERARD H. ROE,[d] AND DARGAN M. W. FRIERSON[a]

[a] *Department of Atmospheric Sciences, University of Washington, Seattle, Washington*
[b] *Polar Science Center, Applied Physics Lab, University of Washington, Seattle, Washington*
[c] *School of Oceanography, University of Washington, Seattle, Washington*
[d] *Department of Earth and Space Sciences, University of Washington, Seattle, Washington*
[e] *Inigo Insurance, London, United Kingdom*

(Manuscript received 30 August 2023, in final form 18 April 2024, accepted 1 May 2024)

ABSTRACT: Atmospheric heat transport (AHT) is an important piece of our climate system but has primarily been studied at monthly or longer time scales. We introduce a new method for calculating zonal-mean meridional AHT using instantaneous atmospheric fields. When time averaged, our calculations closely reproduce the climatological AHT used elsewhere in the literature to understand AHT and its trends on long time scales. In the extratropics, AHT convergence and atmospheric heating are strongly temporally correlated suggesting that AHT drives the vast majority of zonal-mean atmospheric temperature variability. Our AHT methodology separates AHT into two components (eddies and the mean meridional circulation) which we find are negatively correlated throughout most of the mid- to high latitudes. This negative correlation reduces the variance in the total AHT compared to eddy AHT. Last, we find that the temporal distribution of the total AHT at any given latitude is approximately symmetric.

KEYWORDS: Energy budget/balance; Heat budgets/fluxes; Heating

1. Introduction

Zonal-mean meridional atmospheric heat transport (AHT) has long been recognized as important for understanding Earth's hydrologic and energetic balances (e.g., Pierrehumbert 2010; Held and Soden 2006; Siler et al. 2018). Historically, AHT has been used to understand numerous topics including the migration of the intertropical convergence zone (e.g., Kang et al. 2008), the intensity and location of the storm tracks (Shaw et al. 2018), and the degree of polar amplification (Hwang et al. 2011). For these applications, AHT is typically calculated at monthly or longer time scales (e.g., Trenberth and Stepaniak 2003; Donohoe et al. 2020). Meanwhile, an emerging body of the literature has demonstrated the role of synoptic time-scale AHT in driving the variability of sea ice and polar warming (Woods et al. 2013; Laliberté and Kushner 2014; Mortin et al. 2016; Doyle et al. 2011; Cardinale and Rose 2022; Kapsch et al. 2013; Messori et al. 2018; Blanchard-Wrigglesworth et al. 2023) and has advocated that individual events make disproportionately large contributions to the climatological AHT (Woods and Caballero 2016; Messori and Czaja 2013). The method used to calculate AHT at high frequencies differs between studies (Messori and Czaja 2013, 2015; Lembo et al. 2019; Liang et al. 2018), making it difficult to relate the calculations of high-frequency AHT to those of climatological AHT.

In this work, we introduce a new method for calculating AHT at any instant of time. Our methodology is motivated by two goals: (i) to develop a method to accurately calculate AHT at any instant in time that is consistent with existing AHT calculations at longer time scales and (ii) to develop an AHT calculation that is strongly related to the heating of the atmospheric column at 6-hourly to daily time scales and is independent of transient mass imbalances (Liang et al. 2018).

This manuscript is organized as follows. In section 2, we introduce the new AHT calculation, demonstrate that it reproduces more typical AHT calculations (e.g., Donohoe et al. 2020) in the time mean, and present the spatial and seasonal patterns of AHT variability. In section 3, we demonstrate that anomalies in our novel metric of AHT are strongly connected to heating (and moistening) of the atmospheric column. We then compare our new AHT calculation to previous work that calculated only one component of the AHT and to the AHT coming from mass transports in the atmosphere. We find that our new AHT methodology is better correlated with changes in atmospheric temperature and moisture than previous work. In section 4, we examine connections between the two components of our AHT calculation (eddy AHT and and the mean-meridional circulation AHT). We find the two components are negatively correlated, with the strongest correlations in the mid- to high latitudes. Last, we explore the temporal distribution of AHT (section 5).

2. AHT calculation methodology

Here, we develop a new method of calculating AHT from three-dimensional atmospheric fields at any instant in time. We provide a detailed methodology section to illustrate how our calculation compares to that in previous work. The new method allows AHT to be calculated at each instant independently and makes no reference to the time-mean fields aside from the time-mean surface pressure.

Supplemental information related to this paper is available at the Journals Online website: https://doi.org/10.1175/JCLI-D-23-0521.s1.

Corresponding author: Tyler Cox, tyler.tsc@gmail.com

DOI: 10.1175/JCLI-D-23-0521.1

The relevant energetic quantity for calculating AHT is the moist static energy (MSE) defined as

$$\mathrm{MSE} = c_p T + L_v q + gZ, \tag{1}$$

where c_p is the specific heat of air, T is the atmospheric temperature, L_v is the latent heat of vaporization, q is the specific humidity, g is the acceleration due to gravity, and Z is the geopotential height.

With our new AHT methodology, we calculate the net transport of MSE across a latitude band relative to an unchanging atmospheric mass. By using an unchanging atmospheric mass, we remove the impact that nonzero mass fluxes can have on AHT, which can be substantial (Liang et al. 2018; Cox et al. 2023). AHT can thus be thought of as the MSE contrasts between poleward and equatorward moving air, which at a given latitude can be accomplished by two distinct types of circulations: 1) at a given pressure level, zonal anomalies in meridional winds acting on zonal anomalies in MSE (hereafter eddies) and 2) zonal-mean meridional winds at different pressure levels acting on the vertical gradient in MSE (hereafter the mean-meridional circulation or MMC). These two contributions to instantaneous AHT at a given latitude θ are calculated as

$$\text{total AHT} = \frac{2\pi a\cos(\theta)}{g}\int_0^{\overline{P_s}} \left(\underbrace{[v]^{\dagger}[\mathrm{MSE}]^{\dagger}}_{\text{MMC AHT}} + \underbrace{[v^{*}\mathrm{MSE}^{*}]}_{\text{eddy AHT}} \right) dp, \tag{2}$$

where v is the meridional wind, p is the pressure, $\overline{P_s}$ is the time-mean surface pressure, a is the radius of Earth, square brackets [] denote zonal averages, overbars ($\overline{\ }$) denote monthly time averages, asterisks (*) are departures from the zonal average, and swords (†) are departures from the vertical average [see Eq. (6) for details on how the vertical average is calculated]. This AHT calculation method implicitly conserves mass prior to the calculation of the MMC AHT by removing the vertical average v and MSE (Marshall et al. 2014), and requires no further barotropic wind (Trenberth and Stepaniak 2003) or vertically varying energetic (Bangalath and Pauluis 2020) adjustment. If the vertical averages are not removed, the magnitude and variance of the MMC AHT change due to the zonal- and vertical-mean mass flux (section 3).

This method differs from that of Messori and Czaja (2013) who calculated the transient-eddy portion of the AHT from the product of the temporal anomalies, relative to the time mean, in v and MSE at each grid point. Lembo et al. (2019) calculated AHT as a function of wavenumber at each instant. Thus, our eddy AHT is different from that in Lembo et al. (2019) as it comes from zonal anomalies, but our MMC AHT field is identical or very similar to their wavenumber 0 ($k = 0$) field, depending on whether they use the time-mean or instantaneous surface pressure in their calculation. We perform all AHT calculations using instantaneous ERA5 data from 1979 to 2018 that has been interpolated to 37 vertical pressure levels, has 0.5° horizontal resolution, and has 6-hourly temporal resolution (Hersbach et al. 2018). Data from pressure levels greater than $\overline{P_s}$ at each gridpoint are masked out. We primarily focus on the winter seasons in this work, December–February (DJF) in the Northern Hemisphere, and June–August (JJA) in the Southern Hemisphere.

To relate our methodology to the climatological AHT and previous work on the temporal variability of AHT, it is instructive to decompose the eddy fields (v^* and MSE^*) into time-mean stationary eddies (SE; $\overline{v^*}$ and $\overline{\mathrm{MSE}^*}$) and transient eddies (TE; $v^{*\prime}$ and $\mathrm{MSE}^{*\prime}$), where $\prime$ are departures from the time average. The eddy AHT at a given instant and latitude is then

$$\text{eddy AHT} = \frac{2\pi a\cos(\theta)}{g}\int_0^{\overline{P_s}} \left(\underbrace{[\overline{v^*}\,\overline{\mathrm{MSE}^*}]}_{\text{SE AHT}} + \underbrace{[\overline{v^*}\mathrm{MSE}^{*\prime}] + [v^{*\prime}\overline{\mathrm{MSE}^*}]}_{\text{Mixed Terms}} + \underbrace{[v^{*\prime}\mathrm{MSE}^{*\prime}]}_{\text{TE AHT}} \right) dp. \tag{3}$$

To calculate the climatological eddy AHT, we take the time average of Eq. (3) which gives

$$\overline{\text{eddy AHT}} = \frac{2\pi a\cos(\theta)}{g}\int_0^{\overline{P_s}} \left(\underbrace{[\overline{v^*}\,\overline{\mathrm{MSE}^*}]}_{\text{SE AHT}} + \underbrace{[\overline{v^{*\prime}\mathrm{MSE}^{*\prime}}]}_{\text{TE AHT}} \right) dp. \tag{4}$$

Equation (4) is equivalent to Eq. (3) in Donohoe et al. (2020), showing the connection between the standard definitions of AHT and this new calculation methodology.

The time mean of the Mixed Terms in Eq. (3) is 0 because the time-mean terms ($\overline{v^*}$ and $\overline{\mathrm{MSE}^*}$) can be pulled out of the time-averaging operator and the time mean of the transient terms ($v^{*\prime}$ and $\mathrm{MSE}^{*\prime}$) is 0 by definition. Thus, in the time mean, stationary and transient eddies do not interact and the eddy AHT can be decomposed into contributions from the stationary eddies and the transient eddies, which is a result of the temporal covariance between v and MSE in baroclinic eddies (Lorenz 1953).

However, at any instant, the transient-eddy portions of v and MSE ($v^{*\prime}$ and $\mathrm{MSE}^{*\prime}$) can interact with the stationary eddy portions of v and MSE ($\overline{v^*}$ and $\overline{\mathrm{MSE}^*}$) to result in nonzero contributions to the instantaneous eddy AHT by the Mixed Terms. This contribution is associated with the time-mean circulation advecting temporal anomalies in MSE and the anomalous eddy mass transports advecting the time-mean eddy MSE field, respectively. Some previous work on the temporal variability of AHT (Messori and Czaja 2013, 2014, 2015) did not diagnose the impact of the Mixed Terms or stationary eddies on AHT variability and instead focused solely on the transient eddies. We note that there is no a priori expectation as to whether the Mixed Terms will enhance or diminish the temporal variability (or higher order moments) of the AHT distribution. However, if the climatological structures of MSE and v (which contribute to poleward AHT) were amplified (and diminished) in concert over time, we expect the AHT temporal variability would be enhanced by the Mixed Terms. A similar decomposition for the MMC AHT is also possible and is detailed in the online supplemental material.

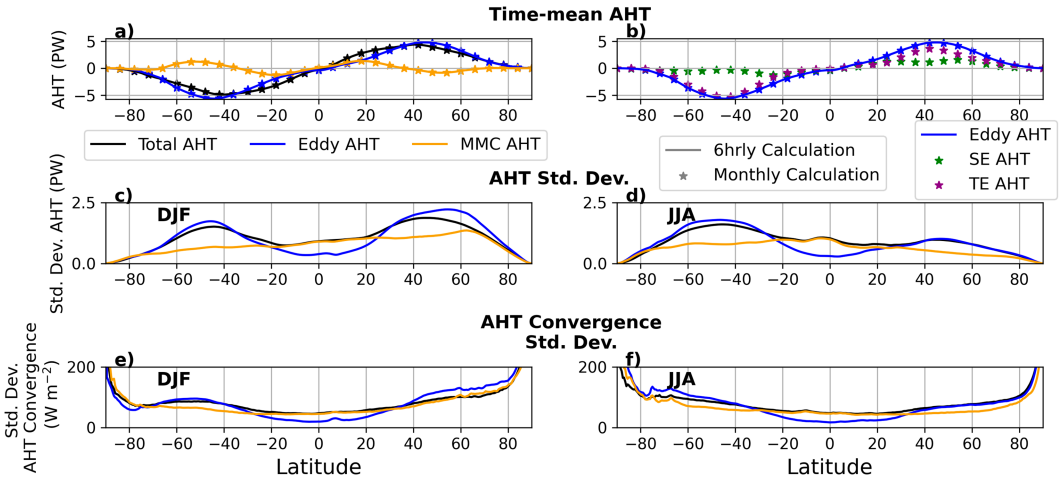

FIG. 1. In (a) and (b), the solid lines show the annual-mean AHT components calculated using our 6-hourly calculation methodology in this study [see Eq. (2)], and the stars show the same annual-mean AHT calculated using the more typical monthly calculations as in Donohoe et al. (2020). The panels demonstrate the good agreement between the two methods. The standard deviation of the total AHT and its components calculated using the 6-hourly methodology in this paper, are shown for DJF in (c) and JJA in (d). The standard deviation of meridional convergence of AHT and its components are shown for DJF in (e) and JJA in (f).

In the time mean, the AHT calculated from Eq. (2) is nearly identical to that derived from more standard AHT calculations (e.g., Donohoe et al. 2020) based on monthly mean atmospheric fields and eddy covariances (Fig. 1a). This is expected given the mathematical decomposition highlighted in Eqs. (3) and (4) and Eqs. (S1) and (S2). While the monthly AHT calculations separate eddy AHT into both a transient and a stationary AHT component, calculating AHT at each instant means we are unable to decompose the eddy AHT into stationary and transient components due to their interaction (e.g., the Mixed Terms).

This new methodology allows us to assess the variability of AHT at 6-hourly time scales (Figs. 1c,d). We find substantial variability, with the standard deviation of the total AHT roughly half its mean value in the mid- to high latitudes. The standard deviation peaks in the midlatitudes and is higher in the winter hemisphere. In the tropics, the variability in the total AHT is dominated by the MMC AHT, while in the extratropics, the variability is dominated by the eddy AHT. In the extratropics, the standard deviation of eddy AHT exceeds the standard deviation of the total AHT at many latitudes (Fig. 1), a topic we explore more in section 4.

3. Connections between AHT and atmospheric energy changes

AHT variability can also be examined through an energetic perspective by evaluating the heating and cooling rates implied by AHT meridional convergence (Figs. 1e,f). The heating and cooling rates coming from AHT meridional convergence can be compared to the rates implied by radiative and surface fluxes and to the actual rates in the atmospheric column. The standard deviation of AHT meridional convergence is near 100 W m^{-2} throughout most of the midlatitudes and peaks near the poles where the zonal circumference approaches 0. The variability of energy convergence from AHT exceeds the variability in radiation and surface heat fluxes by a factor of roughly 3 in the midlatitudes. Therefore, AHT convergence is the dominant driver of atmospheric heating and cooling at 6-hourly time scales at most latitudes (supplemental Fig. 1), with most AHT convergence balanced by storage in the atmospheric column.

We visualize the atmospheric MSE changes associated with AHT by regressing the normalized AHT convergence at 50°N against temperature (and humidity) anomalies at different time lags. The resulting time series (Fig. 2) can be thought of as the typical atmospheric response to a one standard deviation AHT event in the days before (negative lags) and after (positive lags) the event. Strong heating and moistening of the entire troposphere occurs in the days after a meridional convergence of AHT. The vertically integrated anomalies (Fig. 2b) show the warming and moistening of the atmospheric column over a swath of latitudes approximately 15° wide centered on 50°N in the days after the event, lasting approximately 4 days. Latitudes farther north and south of 50°N show slight cooling concurrent with the warming around 50°N. Temperatures at roughly 200 hPa at 50°N show cooling starting near lag-zero and then slowly dissipating (Fig. 2a). We hypothesize that the cooling aloft stems from a rising of the tropopause caused by the warming of the troposphere. We next generalize the connection between meridional AHT convergence and column temperature and moisture changes to all latitudes.

We evaluate how well AHT captures changes in atmospheric temperature and moisture by calculating temporal correlations at each latitude between the AHT meridional convergence and the column-averaged MSE temporal tendency. This can be done for an individual component of AHT and for different AHT methodologies. Correlations closer to

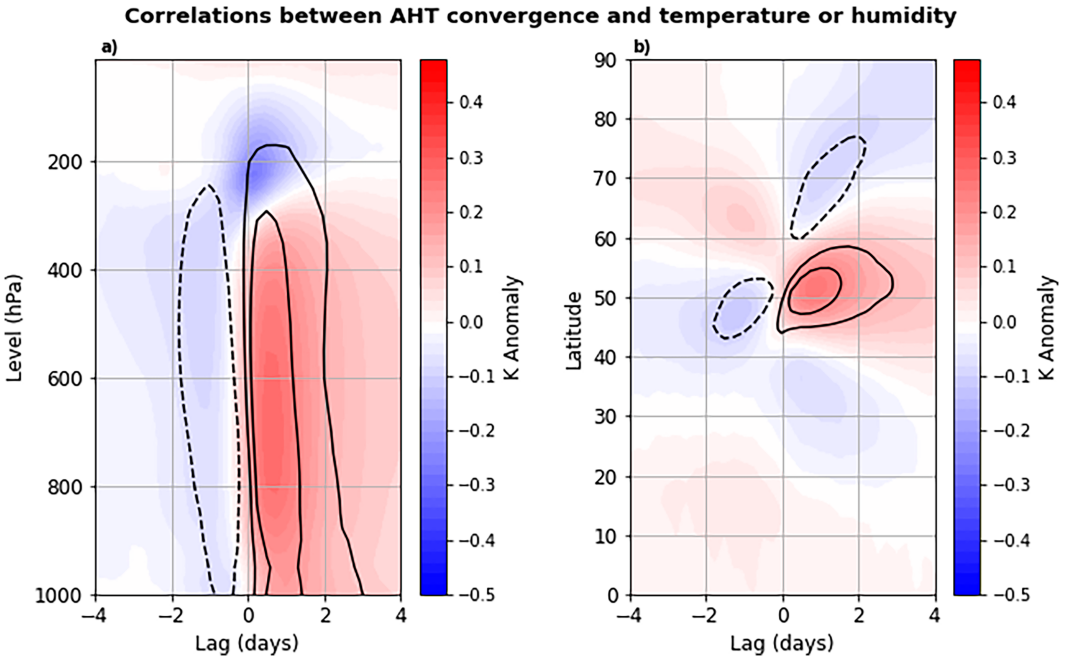

FIG. 2. Temporal evolution of temperature (colors) and humidity (contours) anomalies associated with a one standard deviation AHT meridional-convergence event at 50°N. The plotted values show the normalized lagged regression against AHT convergence at 50°N of (a) the zonal mean at 50°N at various pressure levels and (b) the vertical and zonal mean at various latitudes. Anomalies are calculated as the deviations from the time mean for that day of the year. Black specific humidity contours are 10 g kg^{-1} with the zero contour excluded.

one indicate that the temporal variability in the column MSE is well explained by the variability of the meridional convergence of AHT. We focus on correlations but note that the regression coefficients are near 1 (not shown), implying that the dominant energy balance is between AHT convergence and column MSE changes, whereas atmospheric radiation and surface heat fluxes play a more minor role at these time scales. The TE AHT alone (calculated using the methodology in Messori and Czaja 2013) shows correlations near 0.5 at most latitudes (purple line in Fig. 3a). The full-eddy AHT shows stronger correlations, peaking near 0.8, at all latitudes (blue line in Fig. 3a). The stronger correlations when using the full-eddy AHT show the importance of the SE AHT and the Mixed Terms for explaining atmospheric MSE changes. The total AHT shows still better correlations in the mid- and high latitudes, owing to the inclusion of the MMC AHT (black line in Fig. 3a). However, in the tropics, the total AHT is less correlated with the column MSE tendency than the eddy AHT alone. In the tropics, most of the AHT comes from MMC AHT, and past work has shown that the Hadley cell in ERA5 has issues related to precipitation and latent-heating trend inaccuracies (e.g., Chemke and Polvani 2019). ERA5 also struggles with the magnitude of tropical precipitation (e.g., Hassler and Lauer 2021). We speculate that the weak correlations between the total AHT meridional convergence and the column MSE tendency in the tropics are related to moisture assimilation tendencies in the reanalysis that do not conserve energy. In CESM2 (Danabasoglu et al. 2020), the correlations of the total AHT are near 0.8 at all latitudes including the tropics (supplemental Fig. 2), supporting the idea that inaccurate precipitation in ERA5 may be at fault. Correlations are not equal to 1 partially due to the effects of atmospheric radiation and surface heat fluxes breaking the connection between AHT convergence and column MSE changes (Peixoto and Oort 1992; Adam et al. 2016).

Removing the AHT due to the mass transport is also important for ensuring strong connections between the AHT convergence and the column MSE tendency. The AHT due to the mass fluxes alone, which we remove, can be found by multiplying the zonal- and vertical-mean v with the zonal- and vertical-mean MSE. Mathematically, the AHT due to mass transport is

$$\text{AHT Mass Transport} = \frac{2\pi a \cos(\theta)}{g}([\widehat{v}][\widehat{\text{MSE}}]), \tag{5}$$

where $\widehat{\ }$ is a vertical average and is defined as

$$\hat{X} \equiv \frac{1}{\overline{P_s}}\int_0^{\overline{P_s}}(X)\,dp. \tag{6}$$

The AHT Mass Transport could also be calculated as the mass transport required to balance the surface pressure tendency poleward of each latitude, which produces similar results to Eq. (5).

The total AHT with the AHT Mass Transport included (red line in Fig. 3b) shows much weaker correlations than the total AHT alone (black line in Fig. 3b). The weaker

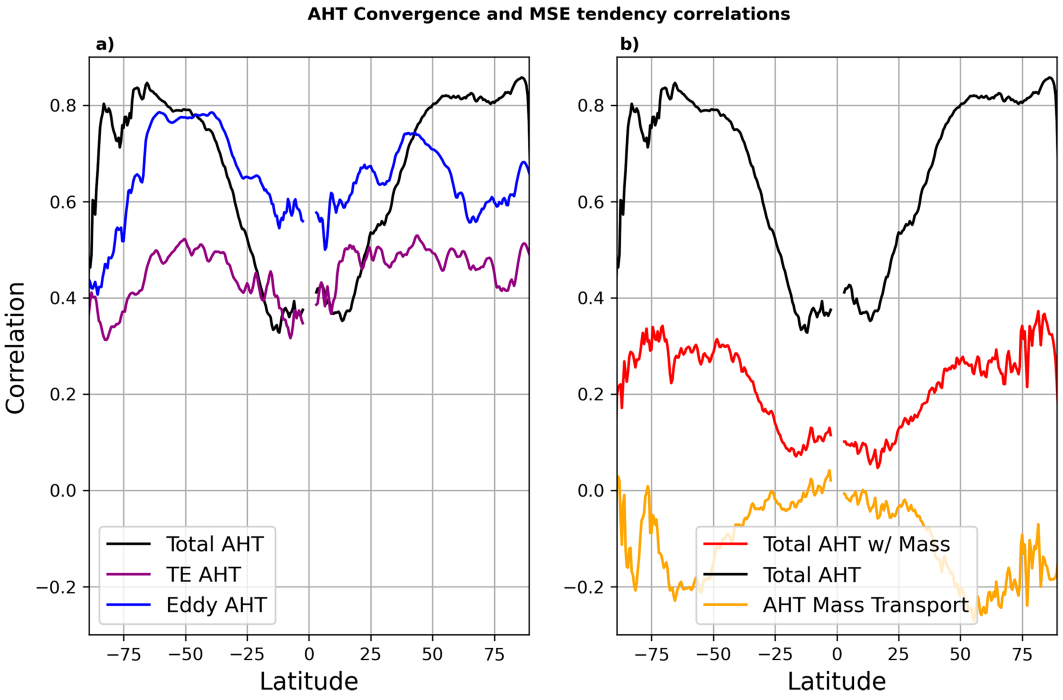

FIG. 3. Temporal correlations between the meridional convergence of various AHT fields and the vertically integrated MSE temporal tendency with DJF data shown in the Northern Hemisphere and JJA data in the Southern Hemisphere. Data within 5° of the equator are masked, and the black total AHT lines are identical in both plots. The TE AHT is calculated as in Messori and Czaja (2013). All data are deseasonalized before correlations are calculated.

correlations when including the mass transport are due to the AHT Mass Transport being uncorrelated (tropics) or slightly negatively correlated with the column MSE tendency (midlatitudes; yellow line in Fig. 3b). We hypothesize that the negative correlation between the AHT Mass Transport meridional convergence and the column MSE tendency is due to the tendency for mass (and thus AHT Mass Transport) divergence under the presence of a thermal low. In other words, when the column is warming, there is a tendency for surface pressure to decrease demanding export of atmospheric mass from the region. Altogether, our AHT methodology shows stronger correlations with the column MSE tendency than alternative definitions of AHT which neglect the mixed eddy terms and mass transport considerations.

In addition to creating weaker connections with the column MSE tendency, calculating only the TE AHT or including the AHT Mass Transport results in substantially different values for the variance of the AHT fields. The TE AHT has a smaller standard deviation than the eddy AHT at all latitudes, showing that the SE AHT and the Mixed Terms work to enhance the variability of the TE AHT alone (Fig. 4). The TE AHT and eddy AHT standard deviations are closer to each other in the Southern Hemisphere than in the Northern Hemisphere, likely because SE AHT plays a more minor role in the Southern Hemisphere (e.g., Donohoe et al. 2020).

The temporal variability of the AHT Mass Transports is larger than the variability in the total AHT (excluding mass transports) at all latitudes, particularly in the tropics (Fig. 1). The large variability in the AHT Mass Transport agrees with previous work that found substantial temporal variability in the AHT if the AHT Mass Transport is not removed (Liang et al. 2018). Given the weak connections between the AHT Mass Transport and atmospheric MSE changes, as well as its enormous temporal variability, we stress that it is vital to perform a mass correction when calculating AHT at any time scale (e.g., Cox et al. 2023).

4. Connections between the MMC and Eddy AHT components

Total AHT is the sum of eddy and MMC AHT, which do not operate independently of one another (e.g., Salustri and Stone 1983; Walker and Schneider 2006; Donohoe et al. 2020; Cox et al. 2022). In the time mean, previous work has found connections between eddies and the MMC in both the midlatitudes (e.g., Salustri and Stone 1983) and subtropics (e.g., Walker and Schneider 2006). The transformed-Eulerian mean (TEM) framework provides expectation that eddy and MMC AHT will counteract each other in the mid- and high latitudes; the generation of momentum fluxes by midlatitude eddies, of course, is also crucial in determining the Ferrel cell (e.g., Wallace et al. 2023).

On shorter time scales, a heat transport in one region forces a regional secondary circulation response. Since a maximum in poleward eddy heat transport causes a reduction in the temperature gradient, an indirect circulation must appear to keep the flow in thermal wind balance; ascent on the poleward side and descent on the equatorward side act to restore

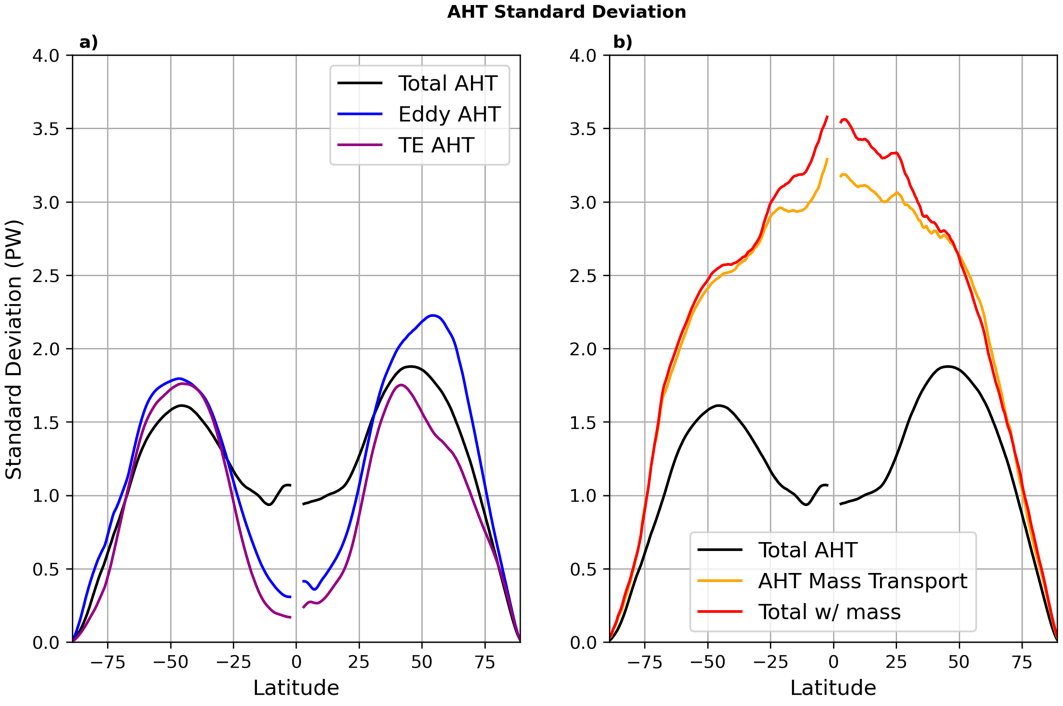

FIG. 4. Standard deviation of AHT and its components with DJF data shown in the Northern Hemisphere and JJA data in the Southern Hemisphere. Data within 5° of the equator are masked, and the black total AHT lines are identical in both plots.

some of the temperature gradient. While this happens regionally, the balances also hold in the zonal mean, and the zonal and time mean of these regional secondary circulations can be thought of as the Ferrel cell. This zonal-mean picture is the one we investigate here, namely, the connection between eddy and MMC AHT on 6-hourly time scales.

To investigate the relationships between the eddy and MMC AHT fields at 6-hourly time scales, we first make composites based on the strongest 5% of eddy AHT events at 50°N during DJF (Fig. 5). The eddy AHT anomalies propagate northward over time at a scale of approximately 10° day^{-1}, as would be expected in midlatitude synoptic-scale storms (colors, Fig. 5a). The MMC AHT has negative anomalies (dashed black lines) that are partially collocated with the positive eddy AHT anomalies (red shading). The near-collocation of the maximum anomalies shows that there is near-zero lag between the two fields. The eddy AHT anomalies are positive and the MMC AHT anomalies are negative, showing compensation between the two AHT components. There is also some indication of positive MMC AHT anomalies toward the edge of the Hadley cell (black contours, Fig. 5a), which are consistent with a temporary strengthening and poleward expansion of the Hadley cell.

The mass-overturning streamfunction anomalies show a strengthening Ferrel cell centered around 50°N and a strengthened and slightly expanded Hadley cell, in line with the MMC AHT anomalies (Fig. 5b). The anomalies in the streamfunction show that the MMC AHT anomalies are indicative of robust changes in the atmospheric dynamics.

We can generalize the relationship between 6-hourly eddy and MMC AHT to all AHT events, not just the extremes, by calculating linear regression slopes between the eddy and MMC AHT data at each latitude during DJF. We use these regression slopes to find correlation coefficients r at each latitude (Fig. 5c). Lagged regressions between the eddy and MMC AHT fields do not result in substantially higher correlation coefficients, suggesting that the connections between the fields happen nearly instantaneously. The regression slopes are negative at latitudes poleward of 20°, indicating that increased poleward eddy AHT is associated with decreased poleward (or more equatorward) AHT by the MMC just as was seen for the extreme eddy AHT event composite in Fig. 5a. In CESM2 (Danabasoglu et al. 2020), slopes are negative at all latitudes, including the tropics (supplemental Fig. 3). We hypothesize that the positive slopes in the tropics in ERA5 in Fig. 5c may be related to the previously mentioned issues with tropical precipitation in ERA5. All the slopes have a magnitude < 1, meaning that, on average, the MMC AHT adjustment only partially compensates for the eddy AHT changes. Slopes peak at a magnitude of around 0.4 in the Northern Hemisphere storm track between 50° and 70°N. A slope of 0.4 implies that total AHT events are only about 60% as large as one would expect from the eddy AHT alone. While calculation methodologies are different, this result is qualitatively similar to that in Lembo et al. (2022).

One result of this negative correlation is that in the mid- and high latitudes, the total AHT has a smaller standard deviation than eddy AHT (1.9 PW vs 2.2 PW at 50°N). This effect

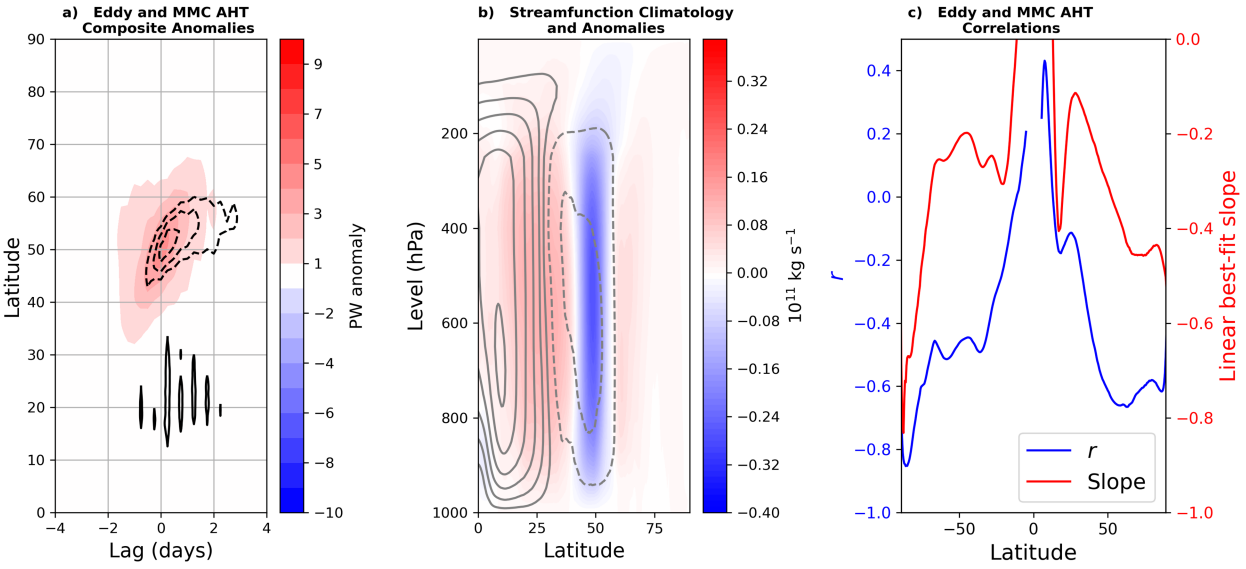

FIG. 5. (a) Composite anomalies for the largest 5% of eddy AHT events at 50°N where colors are the eddy AHT anomalies and black contours are the MMC AHT anomalies where contour intervals are 0.25 PW and contours with a magnitude < 0.75 PW are not shown. Dashed black contours are negative. (b) The mass-overturning streamfunction climatology (gray contours with values of plus and minus 0.1, 0.3, 0.6, 1.0, 1.5, 2.0, and 2.5 10^{11} kg s^{-1}) and anomalies (colors) for the same 5% of events at zero lag. Dashed gray contours are negative. Anomalies are calculated as the deviations from the time mean for that day of the year. (c) Correlations between eddy and MMC AHT with deseasonalized DJF data shown in the Northern Hemisphere and deseasonalized JJA data shown in the Southern Hemisphere. Data within 5° of the equator are masked. The red line shows the slope of the linear regression between MMC and eddy AHT, and the blue line shows the r values based on those slopes.

becomes more noticeable at higher latitudes. Interestingly, the eddy and MMC AHT anticorrelation results in the variance of the total AHT (via the method used in this work) being only slightly larger than that of TE AHT (1.6 PW at 50°N) for the following reason: While the Mixed Terms and SE AHT enhance eddy AHT variance relative to the TE AHT variance, the inclusion of the MMC AHT reduces the variance of the total AHT back toward that of the TE AHT alone.

5. The temporal distribution of AHT

Several previous efforts to quantify the temporal distribution of AHT (Messori and Czaja 2013, 2015; Lembo et al. 2019) suggest that the histogram of AHT at all Northern Hemisphere extratropical latitudes is highly positively skewed with a mode near 0 AHT and some extreme outlier poleward AHT events. Here, we revisit this result by comparing the temporal distribution of AHT calculated by our methodology to the TE AHT calculated as in Messori and Czaja (2013) at each latitude separately. We find that the AHT distributions at any given latitude are visually similar for both TE AHT and total AHT but that the TE AHT distributions have more positive skewness (Fig. 6). The distributions at 70° and 80°N are quite skinny, with large excess kurtosis values. The hemispheric distributions (Figs. 6a,b) appear different with peaks near 0 and long positive tails, in line with previous work (Messori and Czaja 2013, 2015; Lembo et al. 2019, 2022). The hemispheric total AHT distribution has a second peak near 6 PW owing to the inclusion of SE AHT, while the hemispheric TE AHT distribution lacks this second peak. The visually asymmetric hemispheric distribution comes from combining latitudes with different mean AHT values, primarily high latitudes where geometric constraints require that AHT tends toward 0. Despite the visual asymmetry of the hemispheric distributions, their skewness values are similar to those of individual latitudes. The asymmetric hemispheric distribution is not emblematic of the underlying physics of AHT and is instead an artifact of combining AHT data from different latitudes. Eddy and MMC AHT show similar results to total and TE AHT (not shown).

Previous work has used the asymmetric hemispheric AHT distribution (e.g., Figs. 6a,b) as a rationale to focus research more heavily on extreme AHT events. While this may have justification for AHT at individual grid points, zonal-mean AHT at individual latitudes (the AHT quantity examined in this paper that we found to be closely connected to atmospheric heating) is not heavily skewed in its temporal distribution. As a result, we argue that it is important to research what sets the mean and standard deviation of AHT, rather than just focusing on extreme events.

6. Summary and conclusions

In this work, we introduced a new way of calculating AHT at any instant. This new AHT methodology is nearly identical to more typical AHT calculations done at monthly time scales in the time mean (e.g., Donohoe et al. 2020) and is closely connected with changes in atmospheric MSE. We illustrate

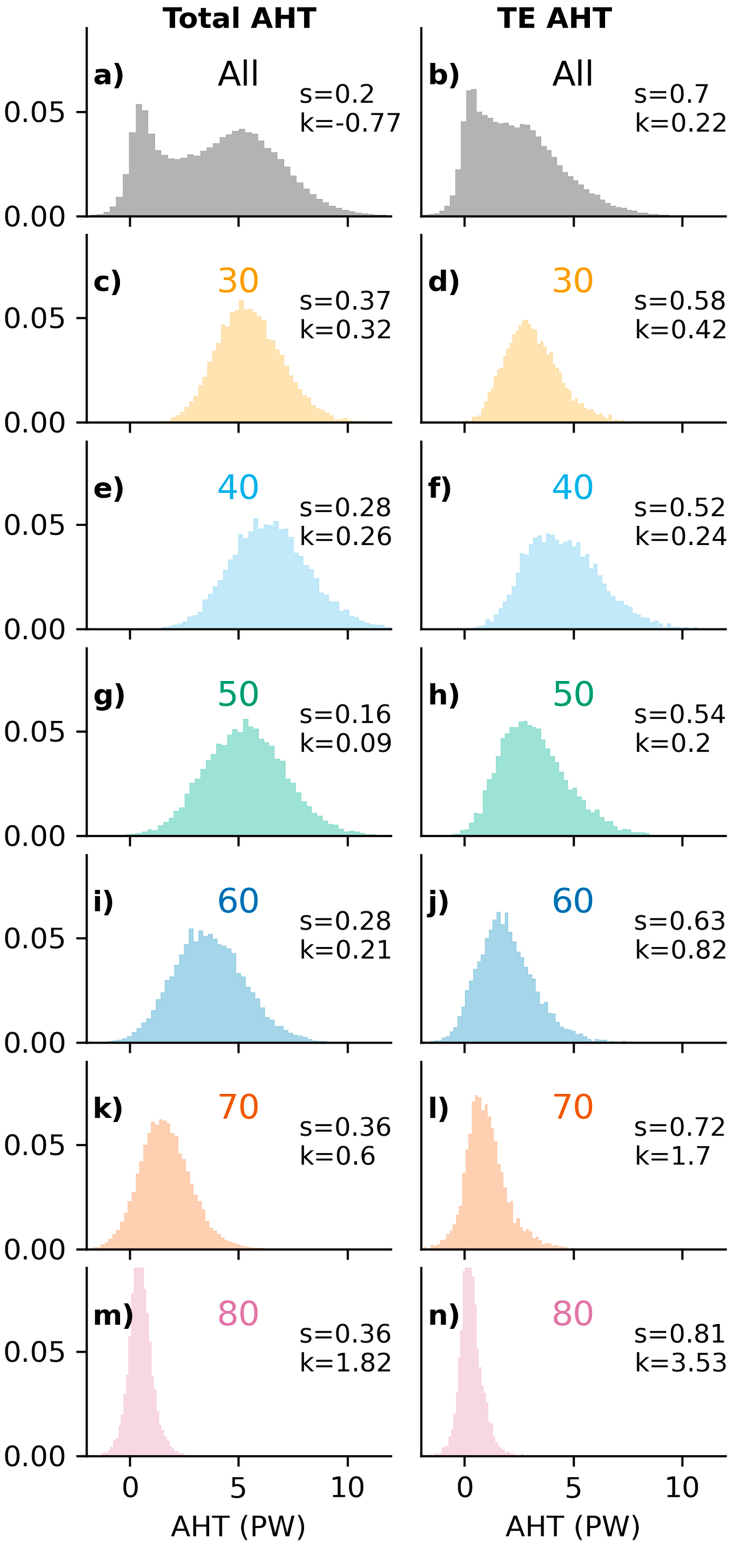

FIG. 6. Probability density functions of (left) total AHT and (right) TE AHT during DJF for (a), (b) the aggregate of plots (c)–(n); (c),(d) 30°N; (e),(f) 40°N; (g),(h) 50°N; (i),(j) 60°N; (k),(l) 70°N; and (m),(n) 80°N. In each plot, the "*s*" number refers to the skewness and the "*k*" number refers to the excess kurtosis. Skewness, the third moment of a distribution, is a measure of asymmetry in the distribution, and excess kurtosis, the fourth moment of a distribution, is a measure of the narrowness of a distribution. Skewness and excess kurtosis are both 0 for a Gaussian distribution.

the importance of correcting the mass budget when calculating AHT, as the AHT coming from the mass transport can be large and is not well correlated with atmospheric MSE variability. This work demonstrates that zonal-mean atmospheric temperature variability is driven primarily by AHT variability. This paves the way for future work using an AHT perspective to investigate model biases in temperature variability, heatwave intensity, and their changes under global warming. A limitation of this framework is that AHT is strongly related to column-integrated atmospheric heating and additional work is required to relate these metrics to surface heating events.

Our new AHT methodology separates AHT into two components: one from the eddy AHT and one from the MMC AHT. We find that these two components are negatively correlated, particularly in the mid- to high latitudes where the MMC AHT associated with the Ferrel cell works to counter eddy AHT. This results in less variance for the total AHT than eddy AHT in the mid- to high latitudes due to the compensating effect of the MMC AHT.

Last, we show that the temporal distributions of AHT, calculated at 6-hourly frequency, are approximately symmetric at individual latitudes. Combining data from different latitudes can obscure this and make the AHT data appear asymmetric. Given the approximately symmetric distributions of AHT at any individual latitude, we argue that focusing on what sets the mean and variability of AHT is more important than focusing solely on extreme AHT events.

Acknowledgments. T. C., A. D., K. C. A., and G. H. R. were supported by the National Science Foundation Award AGS-2019647. A. D. additionally acknowledges the support from AGS-2311540. K. C. A. was additionally supported by a Calvin Professorship in Oceanography.

Data availability statement. All data used in this comment are publicly available reanalysis datasets. Data can be found from ERA5 at https://www.ecmwf.int/en/forecasts/datasets/reanalysis-datasets/era5.

REFERENCES

Adam, O., T. Bischoff, and T. Schneider, 2016: Seasonal and interannual variations of the energy flux equator and ITCZ. Part I: Zonally averaged ITCZ position. *J. Climate*, **29**, 3219–3230, https://doi.org/10.1175/JCLI-D-15-0512.1.

Bangalath, H. K., and O. M. Pauluis, 2020: A new mass flux correction procedure for vertically integrated energy transport by constraining mass, energy, and water budgets. *Geophys. Res. Lett.*, **47**, e2020GL089764, https://doi.org/10.1029/2020GL089764.

Blanchard-Wrigglesworth, E., T. Cox, Z. I. Espinosa, and A. Donohoe, 2023: The largest ever recorded heatwave—Characteristics and attribution of the Antarctic heatwave of March 2022. *Geophys. Res. Lett.*, **50**, e2023GL104910, https://doi.org/10.1029/2023GL104910.

Cardinale, C. J., and B. E. Rose, 2022: The Arctic surface heating efficiency of tropospheric energy flux events. *J. Climate*, **35**, 5897–5913, https://doi.org/10.1175/JCLI-D-21-0852.1.

Chemke, R., and L. M. Polvani, 2019: Opposite tropical circulation trends in climate models and in reanalyses. *Nat. Geosci.*, **12**, 528–532, https://doi.org/10.1038/s41561-019-0383-x.

Cox, T., A. Donohoe, G. H. Roe, K. C. Armour, and D. M. W. Frierson, 2022: Near invariance of poleward atmospheric heat transport in response to midlatitude orography. *J. Climate*, **35**, 4099–4113, https://doi.org/10.1175/JCLI-D-21-0888.1.

——, ——, K. C. Armour, D. M. W. Frierson, and G. H. Roe, 2023: Comment on "moist static energy transport trends in four global reanalyses: Are they downgradient?" by Clark et al. *Geophys. Res. Lett.*, **50**, e2023GL102804, https://doi.org/10.1029/2023GL102804.

Danabasoglu, G., and Coauthors, 2020: The community earth system model version 2 (CESM2). *J. Adv. Model. Earth Syst.*, **12**, e2019MS001916, https://doi.org/10.1029/2019MS001916.

Donohoe, A., K. C. Armour, G. H. Roe, D. S. Battisti, and L. Hahn, 2020: The partitioning of meridional heat transport from the last glacial maximum to CO_2 quadrupling in coupled climate models. *J. Climate*, **33**, 4141–4165, https://doi.org/10.1175/JCLI-D-19-0797.1.

Doyle, J. G., G. Lesins, C. P. Thackray, C. Perro, G. J. Nott, T. J. Duck, R. Damoah, and J. R. Drummond, 2011: Water vapor intrusions into the high Arctic during winter. *Geophys. Res. Lett.*, **38**, L12806, https://doi.org/10.1029/2011GL047493.

Hassler, B., and A. Lauer, 2021: Comparison of reanalysis and observational precipitation datasets including ERA5 and WFDE5. *Atmosphere*, **12**, 1462, https://doi.org/10.3390/atmos12111462.

Held, I. M., and B. J. Soden, 2006: Robust responses of the hydrological cycle to global warming. *J. Climate*, **19**, 5686–5699, https://doi.org/10.1175/JCLI3990.1.

Hersbach, H., and Coauthors, 2018: ERA5 hourly data on single levels from 1979 to present. Copernicus Climate Change Service (C3S) Climate Data Store (CDS), ECMWF, accessed 3 June 2020, https://doi.org/10.24381/cds.adbb2d47.

Hwang, Y.-T., D. M. W. Frierson, and J. E. Kay, 2011: Coupling between Arctic feedbacks and changes in poleward energy transport. *Geophys. Res. Lett.*, **38**, L17704, https://doi.org/10.1029/2011GL048546.

Kang, S. M., I. M. Held, D. M. W. Frierson, and M. Zhao, 2008: The response of the ITCZ to extratropical thermal forcing: Idealized slab-ocean experiments with a GCM. *J. Climate*, **21**, 3521–3532, https://doi.org/10.1175/2007JCLI2146.1.

Kapsch, M.-L., R. G. Graversen, and M. Tjernström, 2013: Springtime atmospheric energy transport and the control of Arctic summer sea-ice extent. *Nat. Climate Change*, **3**, 744–748, https://doi.org/10.1038/nclimate1884.

Laliberté, F., and P. J. Kushner, 2014: Midlatitude moisture contribution to recent Arctic tropospheric summertime variability. *J. Climate*, **27**, 5693–5707, https://doi.org/10.1175/JCLI-D-13-00721.1.

Lembo, V., G. Messori, R. Graversen, and V. Lucarini, 2019: Spectral decomposition and extremes of atmospheric meridional energy transport in the Northern Hemisphere midlatitudes. *Geophys. Res. Lett.*, **46**, 7602–7613, https://doi.org/10.1029/2019GL082105.

——, F. Fabiano, V. M. Galfi, R. G. Graversen, V. Lucarini, and G. Messori, 2022: Meridional-energy-transport extremes and the general circulation of northern hemisphere mid-latitudes: Dominant weather regimes and preferred zonal wavenumbers. *Wea. Climate Dyn.*, **3**, 1037–1062, https://doi.org/10.5194/wcd-3-1037-2022.

Liang, M., A. Czaja, R. Graversen, and R. Tailleux, 2018: Poleward energy transport: Is the standard definition physically relevant at all time scales? *Climate Dyn.*, **50**, 1785–1797, https://doi.org/10.1007/s00382-017-3722-x.

Lorenz, E., 1953: A multiple index notation for describing atmospheric transport processes. AFCRL Rep., 35–53.

Marshall, J., A. Donohoe, D. Ferreira, and D. McGee, 2014: The ocean's role in setting the mean position of the inter-tropical convergence zone. *Climate Dyn.*, **42**, 1967–1979, https://doi.org/10.1007/s00382-013-1767-z.

Messori, G., and A. Czaja, 2013: On the sporadic nature of meridional heat transport by transient eddies. *Quart. J. Roy. Meteor. Soc.*, **139**, 999–1008, https://doi.org/10.1002/qj.2011.

——, and ——, 2014: Some considerations on the spectral features of meridional heat transport by transient eddies. *Quart. J. Roy. Meteor. Soc.*, **140**, 1377–1386, https://doi.org/10.1002/qj.2224.

——, and ——, 2015: On local and zonal pulses of atmospheric heat transport in reanalysis data. *Quart. J. Roy. Meteor. Soc.*, **141**, 2376–2389, https://doi.org/10.1002/qj.2529.

——, C. Woods, and R. Caballero, 2018: On the drivers of wintertime temperature extremes in the high Arctic. *J. Climate*, **31**, 1597–1618, https://doi.org/10.1175/JCLI-D-17-0386.1.

Mortin, J., G. Svensson, R. G. Graversen, M.-L. Kapsch, J. C. Stroeve, and L. N. Boisvert, 2016: Melt onset over Arctic sea ice controlled by atmospheric moisture transport. *Geophys. Res. Lett.*, **43**, 6636–6642, https://doi.org/10.1002/2016GL069330.

Peixoto, J. P., and A. H. Oort, 1992: *Physics of Climate*. American Institute of Physics, 520 pp.

Pierrehumbert, R. T., 2010: *Principles of Planetary Climate*. Cambridge University Press, 652 pp.

Salustri, G., and P. H. Stone, 1983: A diagnostic study of the forcing of the Ferrel cell by eddies, with latent heat effects included. *J. Atmos. Sci.*, **40**, 1101–1109, https://doi.org/10.1175/1520-0469(1983)040<1101:ADSOTF>2.0.CO;2.

Shaw, T. A., P. Barpanda, and A. Donohoe, 2018: A moist static energy framework for zonal-mean storm-track intensity. *J. Atmos. Sci.*, **75**, 1979–1994, https://doi.org/10.1175/JAS-D-17-0183.1.

Siler, N., G. H. Roe, and K. C. Armour, 2018: Insights into the zonal-mean response of the hydrologic cycle to global warming from a diffusive energy balance model. *J. Climate*, **31**, 7481–7493, https://doi.org/10.1175/JCLI-D-18-0081.1.

Trenberth, K. E., and D. P. Stepaniak, 2003: Covariability of components of poleward atmospheric energy transports on seasonal and interannual timescales. *J. Climate*, **16**, 3691–3705, https://doi.org/10.1175/1520-0442(2003)016<3691:COCOPA>2.0.CO;2.

Walker, C. C., and T. Schneider, 2006: Eddy influences on Hadley circulations: Simulations with an idealized GCM. *J. Atmos. Sci.*, **63**, 3333–3350, https://doi.org/10.1175/JAS3821.1.

Wallace, J. M., D. S. Battisti, D. W. J. Thompson, and D. L. Hartmann, 2023: *The Atmospheric General Circulation*. Cambridge University Press, 456 pp.

Woods, C., and R. Caballero, 2016: The role of moist intrusions in winter Arctic warming and sea ice decline. *J. Climate*, **29**, 4473–4485, https://doi.org/10.1175/JCLI-D-15-0773.1.

——, ——, and G. Svensson, 2013: Large-scale circulation associated with moisture intrusions into the Arctic during winter. *Geophys. Res. Lett.*, **40**, 4717–4721, https://doi.org/10.1002/grl.50912.